Electrode positions and current patterns for 3D EIT

Y. Mamatjan[1], D. Gürsoy[2] and A. Adler[1]
[1]Carleton University, Ottawa, Canada
[2]Institute of Medical Engineering, Graz University of Technology, Austria

Abstract: For a 3D electrical impedance tomography (EIT) system, it is necessary to improve electrode geometries placed around a body surface, and correspondingly apply stimulation and measurement patterns to produce maximum distinguishability. Advanced EIT image reconstruction requires designing systems with the electrode geometry and current injection such that the full ensemble of measurements provides as high SNR as possible over all of the volume under investigation not only for over a certain region of interest. A 3D two-electrode plane simulation study is undertaken using 7 electrode geometries and 16 different stimulation and measurement patterns for each electrode geometry. The simulation results show that several electrode geometries and current patterns produced promising results with the high distinguishability which can subsequently lead to improved image reconstruction.

1 Introduction

In Electrical Impedance Tomography (EIT), several publications [1, 2] reported that the linear relationship between global tidal impedance variation and tidal volume cannot be used to calculate end-expiratory lung volume (EELV), since EELV is a global parameter of the whole lung while impedance is measured only at one thoracic level that reflects the impedance variations only in one cross-section of the thorax. Thus, it becomes necessary to develop 3D multiplane EIT to provide more information not only about the regional volume redistribution but also about aeration and ventilation of the whole lung.

The distinguishability of EIT systems is determined by several factors such as current stimulation amplitude, the accuracy of voltage measurement, stimulation and measurement patterns, and the number and placement of electrodes [3]. This paper investigates various electrode geometies combined with different stimulation and measurement patterns. Regarding current patterns, the early consideration on optimizing the drive patterns for EIT was done by [4] using a pair of point drive electrodes approach. Many EIT systems are based on the adjacent voltage measurement as the Sheffield Mark I described by [5] that currents are applied through neighbouring electrodes and the voltages are measured from all remaining adjacent electrode pairs. Various electrode placement strategies within a two-electrode plane were investigated by [6] using only adjacent drive patterns. Recently in [3], we investigated various stimulation and measurement patterns by applying a new distinguishability criterion as a complementary to the previous studies done by [7, 8]. We suggested that the stimulation and measurement patterns separated radially by one electrode less than 180 as the optimal current pattern in a single electrode plane. This new result motivated us to further investigate electrode placement strategies in multiple planes with optimized current patterns to maximize the distinguishability.

In this paper, a 3D simulation was conducted to investigate 7 different electrode geometries with16 different stimulation and measurement patterns (from adjacent to opposite patterns) for each electrode geometry. We simulated each scenario for (i) a single cubic object for in-plane and off-plane, and (ii) two full-height cylindrical objects using a 3D circular Finite Element Model (FEM). We used the formulation for the distinguishability of conductivity targets [3] and applied it for designing electrode positions and finding stimulation and measurement patterns with maximum distinguishability for each electrode position.

2 Methodology

2.1 Distinguishability

We briefly describe the distinguishability formulation in this section but more details can be found in[3]. An EIT system makes a set of transfer impedance measurements from an array of electrodes placed around a body. Most EIT systems apply a set of current patterns k at electrodes to make a set of voltage measurements $\mathbf{v}^k = \mathbf{T}(\boldsymbol{\sigma}_0)\mathbf{c}^k$, where $\mathbf{T}(\boldsymbol{\sigma}_0)$ is the *transfer impedance* matrix of the medium with impedance distribution $\boldsymbol{\sigma}_0$ (in units of Ω). We can define a transfer impedance change $\mathbf{T}_\triangle = \mathbf{T}(\boldsymbol{\sigma}_0) - \mathbf{T}(\boldsymbol{\sigma}_1)$ for a small perturbation $\boldsymbol{\sigma}_1$. Difference imaging was used to produce images of conductivity changes , $\Delta\boldsymbol{\sigma} = \boldsymbol{\sigma}_1 - \boldsymbol{\sigma}_0$ between two states by taking the reference data set ($\mathbf{d_0}$) and further measurements ($\mathbf{d}$) after a certain time interval to provide time-difference measurements $\Delta\mathbf{d} = \mathbf{d} - \mathbf{d_0}$. This method can be applied to image conductivity changes that occur in the human body as a result of physiological functions *i.e* breathing.

Since we generally want to distinguish small changes in conductivity, we linearize around $\boldsymbol{\sigma}_0$ to obtain a conductivity change with a linear function of measurements as $\Delta\mathbf{d} = \mathbf{J}\Delta\boldsymbol{\sigma} + \mathbf{n}$, where $\mathbf{J}$ is Jacobian and $\mathbf{n}$ is zero-mean white Gaussian noise with covariance $\boldsymbol{\Sigma}_n$.

From measurements $\Delta\mathbf{d}$, an impedance change image estimate $\Delta\hat{\boldsymbol{\sigma}}$ is reconstructed from a linearized difference EIT reconstruction algorithm as defined from the norm

$$\Delta\hat{\boldsymbol{\sigma}} = \underset{\boldsymbol{\sigma}}{arg\,min} \|\Delta\mathbf{d} - \mathbf{J}\Delta\boldsymbol{\sigma}\|_{\boldsymbol{\Sigma}_n^{-1}} + P(\boldsymbol{\sigma}), \tag{1}$$

where $P(\cdot)$ represents a penalty or regularization term.

We are interested in the image output $m = A_R\Delta\bar{\sigma}_R$ within a ROI of area A_R with an average impedance change in ROI ($\Delta\bar{\sigma}_R$). In order to *distinguish* $\boldsymbol{\sigma}_1$ from $\boldsymbol{\sigma}_0$, we must reject the null hypothesis H_0: $m = 0$. The probability of H_0 is based on the z-score, which may be further calculated as

$$z = \frac{\bar{m}}{\sigma_m} = \frac{A_R\Delta\bar{\sigma}_R}{\left(\mathbf{R}_R^t\boldsymbol{\Sigma}_n\mathbf{R}_R\right)^{\frac{1}{2}}} = A_R\Delta\bar{\sigma}_R\sqrt{\mathbf{J}_R^t\boldsymbol{\Sigma}_n^{-1}\mathbf{J}_R} = \sqrt{\Delta\mathbf{d}\boldsymbol{\Sigma}_n^{-1}\Delta\mathbf{d}} = \|\Delta\mathbf{d}\|_{\boldsymbol{\Sigma}_n^{-1}}$$

where $\mathbf{J}_R = \frac{1}{A_R}\mathbf{J}$, since we require $\Delta\mathbf{d} = \mathbf{J}_R m$ for changes in the ROI.

The proposed formulation for the distinguishability [3] in terms of a hypothesis test shows that distinguishability is a product of impedance change amplitude, measurement strategies and the inverse of noise amplitude. In this paper we aim to maximize the distinguishability by investigating various combinations of electrode placement strategies, and stimulation and measurement patterns.

2.2 Simulation

EIDORS [9] was employed for simulating electrode geometries and current patterns. A tank phantom in Fig. 1 was modelled for all the simulations. The EIT model has been reconfigured to calculate the Jacobian using Netgen by simulating current patterns and measuring signals from corresponding electrodes.

Electrode geometries and current patterns: A cylinder (30 cm height and 28 cm of diameter) is encircled by 2-plane 8 electrodes which are positioned with the equal distance to middle of the cylinder with the distance of 4 cm between two electrode layers as shown in Fig. 1. All distances are normalized to the height of the cylinder. We investigated 7 electrode placement (EP) strategies: Planar, Planar-offset, Planar-opposite, Zigzag, Zigzag-offset, Zigzag-opposite and Square proposed by [6] for an adjacent pattern and we extended them with 16 different injection and measurement patterns for each EP.

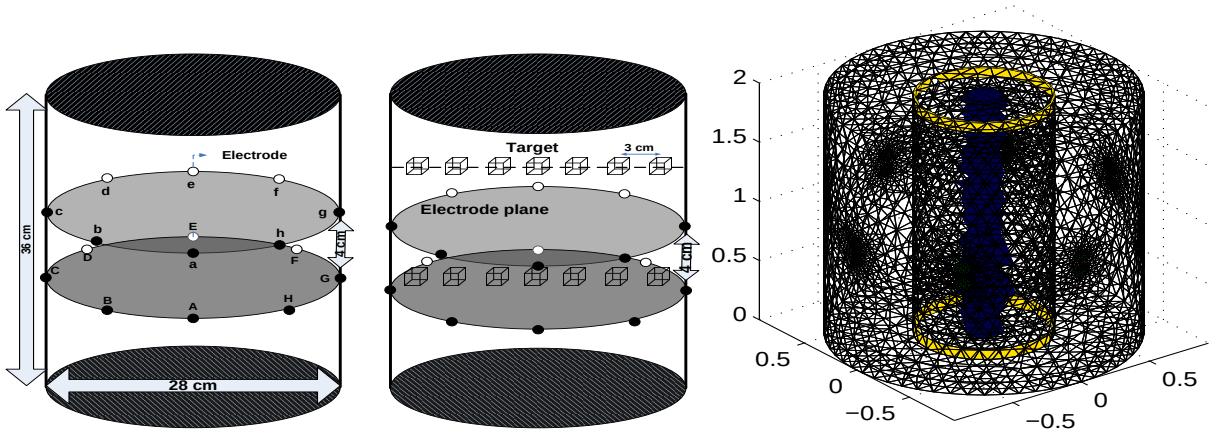

Figure 1: A diagram of *left*: Planar electrode configuration with two-layer 16 electrodes, *middle*: a single cubic object moving horizontally in two vertical planes, *right*: two cylindrical targets with the same volume spaning the full height of the cylindrical volume (2.5 D).

The objective is to select a combination of such an electrode geometry with current patterns that the full ensemble of measurements provides high z value not only in a limited region of interest but also near areas in and out of electrode plane for impedance measurement. A diagram of electrode placement configuration for Planar electrode configuration is shown in Fig. 1:*left*. For the offset arrangement, the lower plane electrodes were rotated to be positioned at the half inter-electrode distance. For each EP and simulation protocol, a sequence of current patterns is injected and voltages are measured to form a data set, where separate electrodes are used for stimulation and measurement.

Stimulation ($\Delta_s = 1, ..., 8$) and measurement ($\Delta_m = 1, ..., 8$)patterns are defined by the distance between the two active electrodes for the stimulation or measurement function and labled as Δ_{sm}. In this study we considered equal stimulation and measurement patterns (Δ_s=Δ_m). For the two-layer electrodes, the adjacent or opposite stimulation is depend on the electrode geometry and current injection patterns unlike a single-layer electrodes in [3], so it should be noted that current pattern Δ_{11} is an adjacent stimulation and measurement pattern for Planar, Planar-offset, Zigzag, Zigzag-offset, and Square geometries, while Δ_{11} is an opposite pattern for Planar-opposite and Zigzag-opposite geometries. Δ_{44} is an opposite pattern for Planar, Planar-offset, Zigzag, Zigzag-offset, and Square geometries.

Simulation models: Two different simulation models were used based on (i) a single cubic object and (ii) two cylindrical objects with full-height perturbation. The background conductivity is 1 S/m and the target conductivity is 0.005 S/m. For (i), the simulation was performed by moving a target of 50 ml in two different vertical planes for 14 horizontal positions in the tank (Fig. 1:*middle*) with 3 cm steps. First vertical plane for the object is set in between two electrode planes, which we call the *central-plane* and the second vertical plane is 6 cm above the *central-plane* (Fig. 1:*middle*).

For (ii), two cylindrical objects of the same volume in 2.5 D span the full height of the tank. A central object is fixed in the center and the other outer object, wrapped around the central object, is expanded with 2 cm steps to 5 different sizes of radius without changing total volume in Fig. 1:*right*. For the distinguishability of two objects, distinguishability values for simulation were calculated directly using the distinguishability criteria formulated in section 2.1 taking into account the average distinguishability values. It is a measure of the

ability of EIT to reliably distinguish structural details of targets, and specifically whether the same volume target is present as two objects or one.

3 Results and discussions

The results of distinguishability for 7 electrode geometries and 16 current patterns are shown in Fig. 2. We calculated the average values of detectability for different target positions in each case. Although we simulated all the combinations of stimulation and measurement patterns, we present representative results with equal number of stimulation and measurement patterns Δ_{sm}. The stimulation and measurement patterns for Planar-opposite and Zigzag-opposite geometries were rearranged to make their z values easy to compare with other configurations, and were renamed to Planar-interleaved and Zigzag-interleaved geometries.

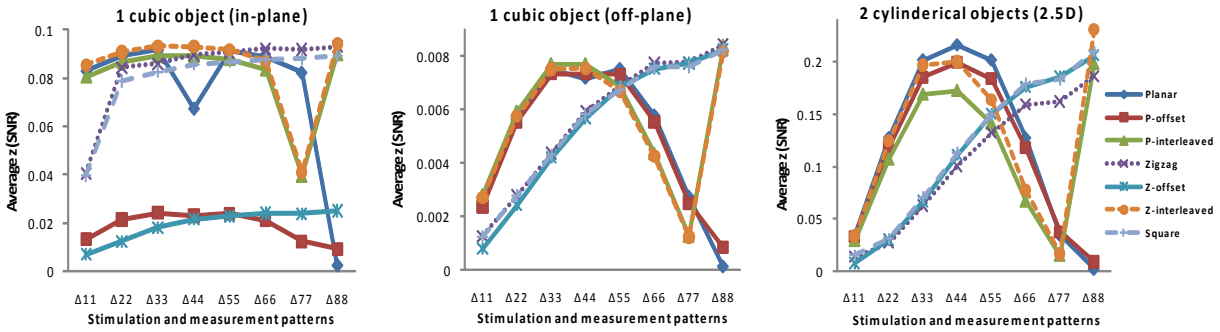

Figure 2: Average distinguishability values for 7 electrode geometries and 16 current patterns. *left*: a cubic object moved horizontally in the *central plane*, *middle*: a cubic object moved horizontally in *off-plane*, *right*: two full-height cylindrical objects (2.5 D). Each distinguishability value is the average value at 7 target positions.

Fig. 2 shows that different Δ_{sm} produced significantly different z values for all electrode geometries. It was observed that Zigzag and Square, Planar-interleaved and Zigzag-interleaved geometries produced the similar results and high distinguishability values for Δ_{88}. Zigzag, Zigzag-offset and Square geometries provided similar characteristics with increasing z value from Δ_{11} to Δ_{88} for off-plane effect with 1 and 2 objects. Planar and Planar-offset geometries have large off-plane effect. Thus, Zigzag, Square and Planar-interleaved configurations with Δ_{88} are considered to offer good performance while Zigzag-interleaved provides the best overall performance for EIT systems with a two-ring electrode phantom system.

In the future work, we will investigate varying distances between the 2 electrode layers and evaluate selected electrode configurations with a real measurement system.

4 References

[1] Bikker IG, Leonhardt S, Bakker J, *et al. Intensive Care Med* 2009; 35: 13621367.
[2] Hinz J, Hahn G, Neumann P, *et al. Intensive Care Med* 2003; 29: 3743.
[3] Adler A, Gaggero PO and Maimaitijiang Y, 2011, *Physiol. Meas.*, In press.
[4] Seagar A D 1983 *PhD Thesis University of Canterbury, Christchurch.*
[5] Brown B H and Seagar A D 1987 *Clin. Phys. Physiol. Meas.* 8, Suppl. A, 91-97.
[6] Graham B and Adler A, *Physiol. Meas.* 28 (2007) S29S44.
[7] Isaacson D 1986 *IEEE T Med Imaging* 5:91-95.
[8] Lionheart WR, Kaipio J, McLeod CN 2001, *Physiol. Meas.* 22 85-90.
[9] Adler A and Lionheart WRB, *Physiol. Meas.* 27:S25-S42, 2006.